Marine and Petroleum Geology 104 (2019) 259–269

Contents lists available at ScienceDirect

Marine and Petroleum Geology

journal homepage: www.elsevier.com/locate/marpetgeo

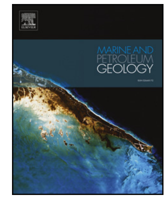

Research paper

Effect of bioturbation on petrophysical properties: Insights from geostatistical and flow simulation modeling

Hassan A. Eltom*, Eugene C. Rankey, Stephen T. Hasiotis, Reza Barati

Kansas Interdisciplinary Carbonate Consortium, Department of Geology, The University of Kansas, 1475 Jayhawk Blvd, Lawrence, KS, 66045, USA

ARTICLE INFO

Keywords:
Bioturbated reservoirs
Multipoint statistic modeling
Super k
Thalassinoides
Burrow connectivity
Dual porosity reservoir

ABSTRACT

As observed in many outcrops and cores, *Thalassinoides* burrow networks (TBN) within *glossifungites* surfaces can be important for permeability enhancement, because the coarse-sediment infill provides permeable pathways in otherwise less permeable media. To explore the effect of bioturbation on reservoir quality, this study uses geostatistical models and fluid-flow-simulation models of TBN and burrow medium (matrix) of hypothetical TBN-bearing strata. Analysis of these models reveals a well-connected burrow network can occur in strata of as little as 12% burrow intensity, and burrow connectivity increases nonlinearly with increases in burrow intensity. Numerical flow simulations of TBN models indicate that gas production cumulative (GPC) controlled primarily by TBN connectivity and matrix permeability. With an impermeable matrix, production occurs through TBN (50 mD average permeability), starts only at burrow intensity of 30%, and GPC increases linearly with burrow intensity. With a permeable matrix (5 mD average permeability), and low permeability contrast between matrix and TBN (one order of magnitude) production starts at relatively low TBN intensity (4%), and GPC increases nonlinearly with burrow intensity. The interaction between matrix and TBN seems to connect more isolated TBN bodies, and increase GPC, and likely help the gas diffusion from matrix through TBN. The fluid flow simulation also illustrates the likelihood of the presence of permeability that drives early water breakthrough (super k) at burrow intensity > 50%. The results advance quantitative understanding of the impact of burrow connectivity on fluid flow properties of TBN-bearing strata and provide a workflow that can be used to model other burrow morphologies to understand their impact on flow properties of bioturbated reservoirs.

1. Introduction

Although the general notion that biological reworking can enhance petrophysical properties of a sedimentary deposit is well established (Pemberton and Gingras, 2005; Gingras et al., 2012; La Croix et al., 2012; Baniak et al., 2015; Bayet-Goll et al., 2017; Leaman and McIlroy, 2017), quantitative understanding of the relationships among burrow intensity, burrow connectivity, and impact on hydrocarbon production is less well constrained. Yet, many hydrocarbon reservoirs and water aquifers are bioturbated. Well-studied bioturbated reservoirs include the Arab-D of the Middle East (Meyer et al., 2000; Pemberton and Gingras, 2005; La Croix et al., 2012), the *Ophiomorpha*-dominated ichnofabric of the Biscayne aquifer, southeastern Florida (Cunningham et al., 2009), the burrow-associated dolomites in the Upper Devonian Wabamun Group of central Alberta (Baniak et al., 2013), and the bioturbated sandstone of the Upper Jurassic Ula Formation of the Norwegian North Sea (Baniak et al., 2015).

Geostatistical modeling and fluid flow simulation provide means to enhance understanding of the impact of burrow intensity and connectivity on reservoir quality of bioturbated strata. Previous geostatistical modeling and fluid flow simulation efforts focused on bioturbated reservoirs have examined the relationship between petrophysical properties of burrow and matrix, and how these impact fluid flow (e.g., Gingras et al., 2012; La Croix et al., 2012; Baniak et al., 2013). These studies have established the concept of the dual-permeability and dual-porosity fluid flow media that occurs within bioturbated reservoirs. Dual-permeability fluid flow media include a high contrast in permeability between the matrix and burrows, empirically estimated to be three orders of magnitude difference (Gingras et al., 2012). Systems with such marked permeability contrasts between the matrix and burrows will favor preferential fluid flow through burrows, with subsidiary diffusive fluid flow from the matrix to the burrow network. In the dual-porosity fluid flow media there is a low contrast in permeability between the matrix and burrows. Gingras et al. (2012) set a value of one order of magnitude difference in permeability for the dual-porosity fluid flow media. If such permeability contrasts occur between the

* Corresponding author.
E-mail address: heltom@ku.edu (H.A. Eltom).

https://doi.org/10.1016/j.marpetgeo.2019.03.019
Received 17 April 2018; Received in revised form 12 March 2019; Accepted 13 March 2019
Available online 19 March 2019

matrix and burrows, fluid flows similarity through burrows and matrix.

We introduce in this paper a new workflow for modeling burrows and bioturbated strata to understand their effective flow properties. The new workflow centers around building a realistic morphology of burrows using multipoint statistics (MPS) in high-resolution geocellular models to provide a realistic and accurate representation of bioturbated reservoirs. In this context, the objectives of this study are to: 1) construct geologically realistic three-dimensional (3D) models of *Thalassinoides* burrow networks (TBN) using MPS and petrophysical models (using facies-based property modeling); and 2) use these to understand the impact of burrow intensity on connectivity and fluid flow. The results bear on geological studies of bioturbated reservoirs (particularly *glossifungites* surfaces, Pemberton and Gingras, 2005), reservoir modeling, flow simulation, and ultimately, improvement of hydrocarbon exploration and development strategies in bioturbated strata.

2. Methods

To develop realistic models of TBN, this study utilizes insights from previous work which describe TBN attributes (e.g., Ekdale and Bromley, 1984; Pemberton and Gingras, 2005; Gingras et al., 2012; Jin et al., 2012; La Croix et al., 2012; Rodríguez-Tovar et al., 2017; Eltom and Haisotis, 2019). In this light, the workflow of this study consists of three steps. 1) Generate 3D geological and petrophysical models of a 1 m^3 volume of TBN using Petrel™2016 to understand how burrow intensity impacts TBN connectivity and stratal petrophysical properties. 2) Sequentially upscale the 3D geological and petrophysical models to understand how TBN geometry changes with cell size of the 3D models, and to select an appropriate upscaled model for fluid-flow simulation (a model with the lowest number of cells that preserves the geometry of TBN). 3) Perform fluid-flow simulation using Eclipse-Petrel™2016 to understand the impact of TBN intensity and connectivity on fluid flow.

2.1. 3D geological and petrophysical models

Step one includes building geologically realistic models for burrow networks using MPS. Initially, we constructed a 3D grid of 1 m^3 volume, consisting of cells of 2D horizontal dimensions of 0.3 cm × 0.3 cm, and vertical dimension of ~0.5 cm, in 150 layers, for a total of ~16 × 10^6 cells. This grid was populated by two generic facies: 1) background mud-dominated facies, and 2) grain-dominated TBN. The TBN patterns initially were generated manually within the 3D grid using the paintbrush and pen tools in Petrel™2016. The TBN pattern was shaped by drawing horizontal and vertical cylinders of diameters from ~0.7 to 4.5 cm. These cylinders have boxwork patterns and joints that branch at 60°, 120°, and 180° angles, with similar pattern in vertical and horizontal dimensions (e.g., Ekdale and Bromley, 1984; Pemberton and Gingras, 2005; Gingras et al., 2012; Jin et al., 2012; La Croix et al., 2012; Rodríguez-Tovar et al., 2017; Eltom and Haisotis, 2019).

Using this 3D grid, we generated a training image characterized by Droser and Bottjer (1986) ichnofabric index (ii) of 3. Bioturbation intensity of ~16% is the percentage of bioturbation intensity calculated as the volume of the TBN in the 1 m^3 model. This percentage was chosen to allow construction of a relatively complete model of the 3D boxwork morphology of *Thalassinoides* in horizontal and vertical space from which smaller and greater ii could be modeled. To consider a broader range of ii variability, 15 3D TBN models generated using MPS incrementally increased the density of TBN from 2 to 20% (ii2, ii3), with 2% bioturbation intensity steps, and from 20% (ii3) to 70% (ii5) with 10% bioturbation intensity steps. For example, a 10% TBN burrow model includes a 0.1 m^3 volume of burrow in the model, or around ~16 × 10^5 cells, of total number of cells in the model, which is ~16 × 10^6. Varying TBN burrow intensity permitted evaluation of changes in burrow connectivity with variation of burrow density.

Porosity and permeability were distributed throughout the 3D models using a facies-based distribution, yielding porosity and permeability models mimicking TBN-bearing strata. The distribution occurred separately for each facies (i.e., as designated in the Petrel model; not actual lithofacies), the TBN and the medium, although both used the Gaussian random function simulation (GRFS) algorithm in Petrel™2016. The inputs required for this function are the range of the simulated porosity and permeability (minimum and maximum values), the mean, and the standard deviation. GRFS uses these values as constraints to stochastically distribute porosity and permeability in each facies. The modeled TBN infill and medium values were taken to be similar in composition and texture to those facies in the Arab-D reservoir: skeletal peloidal grainstone for infill, and massive mudstone for the medium. Thus, the TBN and medium of models are populated with petrophysical attributes similar to skeletal peloidal grainstone and massive mudstone of the Arab-D reservoir (Meyer et al., 2000). Accordingly, the TBN was assigned porosity between 30% and 40% (mean = 35% ± 2%) and permeability between 15 and 100 mD (mean = 50 ± 20 mD), and the medium was assigned porosity between 1% and 5% (mean = 2% ± 2%) and permeability between 2 and 10 mD (mean = 5 ± 2 mD).

The connectivity of the resultant TBN models evaluated using the volume calculation tool in Petrel™2016. This tool defines each connected TBN volume as a single body and calculates the abundance (as a % of the total volume of TBN) in the 3D grid. In the model, all volumes of TBN are filled with the same materials (e.g., peloids, skeletal grains, coated grains), and hence they include the same permeability distribution. The 3D grid also is free of any geological features that could compartmentalize TBN bodies (e.g., healed fractures).

2.2. Upscaling the 3D geological and petrophysical models

Upscaling is the procedure of generating a coarser grid from a finer grid; herein finer grid is defined as the geological and petrophysical models constructed in step one of the modeling process. Upscaling is essential for flow simulation (step three) because it reduces the time and effort for simulation runs. This procedure included two major steps: 1) upscaling the 3D grid; and 2) transferring petrophysical properties to the upscaled grid. The downside of the upscaling process is that many of the fine details generated for the TBN in the high-resolution geological and petrophysical models (step one) will be lost if a large cell size (larger size than the geometry of TBN) is used in the 3D grid upscaling. Thus, an appropriate upscaled 3D grid for the 1 m^3 TBN models should be selected for fluid flow simulation (step three). This appropriate 3D upscaled grid is the one with minimum cell size that preserved the TBN geometry.

To select such an appropriate upscaled 3D grid, 10 sequentially upscaled models (Upscaled Models 1–10, Table 1) successively

Table 1
Grid characteristics of the TBN model before upscaling and the 10 sequential upscaled models.

Grid	Size of the model	Total number of cells	number of cells in XYZ directions
Grid before Upscaling	1 m^3	1,67,33,400	334 × 334 x 150
Upscaled Grid 1	1 m^3	40,00,000	200 × 200 x 100
Upscaled Grid 2	1 m^3	10,00,000	100 × 100 x 100
Upscaled Grid 3	1 m^3	2,50,000	50 × 50 x 100
Upscaled Grid 4	1 m^3	1,25,000	50 × 50 x 50
Upscaled Grid 5	1 m^3	20,000	20 × 20 x 50
Upscaled Grid 6	1 m^3	1,000	10 × 10 x 10
Upscaled Grid 7	1 m^3	500	10 × 10 x 5
Upscaled Grid 8	1 m^3	250	5 × 5 x 10
Upscaled Grid 9	1 m^3	125	5 × 5 x 5
Upscaled Grid 10	1 m^3	1	1 × 1 x 1

increased the cell size, reducing a total number of cells in the 3D grid of the 1 m^3 (Table 1) until the grid achieves the coarsest point, in which the model consists of only one cell (Upscaled Model10). After constructing these 10 upscaled 3D grids, the permeability and porosity values from the initial model (fine cells, high-resolution) were transferred to each one of the 10 upscaled grids using scale-up properties process in Petrel. Upscaled permeability values used flow-based methods, which involves performing a numerical pressure simulation on the fine cells of the geological and petrophysical model before upscaling, and using these data to calculate permeability in X, Y, and Z direction. Porosity values were upscaled using the averaging method.

After transferring petrophysical properties in the 10 upscaled grids, we evaluated the preservation of TBN geometry in these ten upscaled grids visually and statistically. Visually, the model lost TBN geometrical details if the TBN fused entirely in the burrow matrix and lost the details of the burrow geometery. Statistically, measuring the range and variance of the permeability in each model of the ten 3D upscaled grids provides an objective means to describe degree of homogeneity between TBN and burrow matrix. The lower the value of the variance and range, the higher the degree of homogeneity between the TBN and matrix. On the basis of these two criteria, we selected the appropriate model for the flow simulation, the model with lowest number of grid cells that preserved the TBN geometry.

2.3. Fluid flow simulation parameters

In step three, a flow simulation applied the black-oil simulator (Eclipse100) in Eclipse-Petrel™2016 on the 1 m^3 models of the selected upscaled 3D grid (Table 2). The models are assumed to have no flow boundary conditions on the top and sides, and contain gas and water, with the gas-water contact placed at 75 cm below the top. A vast constant aquifer provides pressure support of the models at the bottom. The production from flow simulations was from a single 1-m vertical well placed in the center of the model was perforated in the top 10 cm. To match such a small-scale 3D model (1 m^3) with such small cell size (< 1 cm), the completion parameters of this well are set to be a user-defined, bore-hole diameter of 0.004 m, liner and casing diameter of 0.0037 m. Flow rate of one standard cubic meters (SM^3)/Day was used as single control model for this well. Other parameters of flow simulation kept as the default values of Eclipse-Petrel™2016.

Table 2
Parameters used for fluid flow simulation.

Reservoir	Fluids	Gas-water reservoir
	Initial water saturation	0.2
	Initial volumetric factor	0.0053
	Dimension	1 m^3
Contact	Type	Gas water contact
	Pressure	200 bar
	Datum	75 cm below the top of the model
	Datum pressure	0 bar
Fluid Model	Type	Black oil (Eclipse100)
	Sub type	Dry Gas
Reservoir condition	Minimum pressure	80 bar
	Maximum pressure	350 bar
	Reference pressure	215 bar
	Minimum temperature	80 C
Rock physics functions	Saturation	Gas and water (default values in Petrel)
	Compaction	Consolidated limestone (default values in Petrel)
Aquifer	Pressure	Constant pressure head water
	Direction	Bottom up
Production well	Configuration	Vertical well
	Total depth	1 m
	Bore-hole diameter	0.004 m
	Casing dimeter	0.0037 m
	Perforation interval	Upper 10 cm
	Production rate in the well	1 SM3/day

Gas-in-place (GIP) of each simulation model was calculated using the following equation:

$$GIP = m^3 * \text{Grid porosity} * [1\text{-}S_w] * 1/B_g$$

m^3: 1-m cube (the volume of the model)
S_w: water saturation
B_g: gas formation volume factor

The initial gas water saturation of the model is 0.2, whereas the initial gas formation volume factor is 0.0053. These two parameters are dynamic and change through time with production and pressure drop. Eclipse-Petrel™2016 takes into account this dynamic change and calculates the change of these parameters through time. The recovery factors of gas from these specified parameters are > 80%. Considering the small size of the model (1 m^3) we assume that this recovery factor can be significantly different in real-world gas reservoirs.

2.4. Simulation conditions

Keeping simulation parameters constant, we ran fluid flow simulation on 15 simulation cases representing the 15 models of the TBN burrow intensity (burrow intensity range of 2%–70%). In each case, the simulation was run until water breakthrough in the well. Cumulative production, bottom hole pressure, and flow rate in each simulation case were compared among the intensities of TBN to understand the impact of burrow intensity on gas flow.

The 15 simulation cases used porosity and permeability models that were constructed in step one, under three conditions:

1) In condition 1: the porosity of the TBN was switched off (TBN assigned 0% porosity) to ensure that the gas flow exclusively comes from burrow matrix,
2) In condition 2: the porosity of the burrow matrix was switched off (burrow matrix assigned 0% porosity) to ensure that the gas flow exclusively comes from the TBN, and
3) In condition 3: both TBN and matrix porosity were enabled to ensure that gas production comes from both TBN and burrow matrix.

Investigating these three conditions of the 15 fluid flow simulation cases (total of 45 simulation case), allowed a systematic study of the role of petrophysical properties of the burrow matrix and TBN as two end members on effective flow of TBN bioturbated beds.

3. Results

3.1. Similarity of TBN 3D models to the stratigraphic record

The patterns of the TBN connectivity in the models are qualitatively similar to the connectivity of TBN in real-world examples (Figs. 1 and 2). For instance, a 3D view of TBN from the Birdsall Calcareous Grit Member of the Coralline Oolite Formation (Upper Jurassic, Oxfordian) (Fig. 1A) is strikingly similar to modeled TBN (Fig. 1B). Another example from the stratigraphic record (Upper Devonian Wabamun Group, Pine Creek gas field, central Alberta, Canada) shows TBN patterns similar to the TBN model (Baniak et al., 2013). 2D helical CT scans of core from the Wabamun Group (Fig. 2A–C) compare well to 2D slices

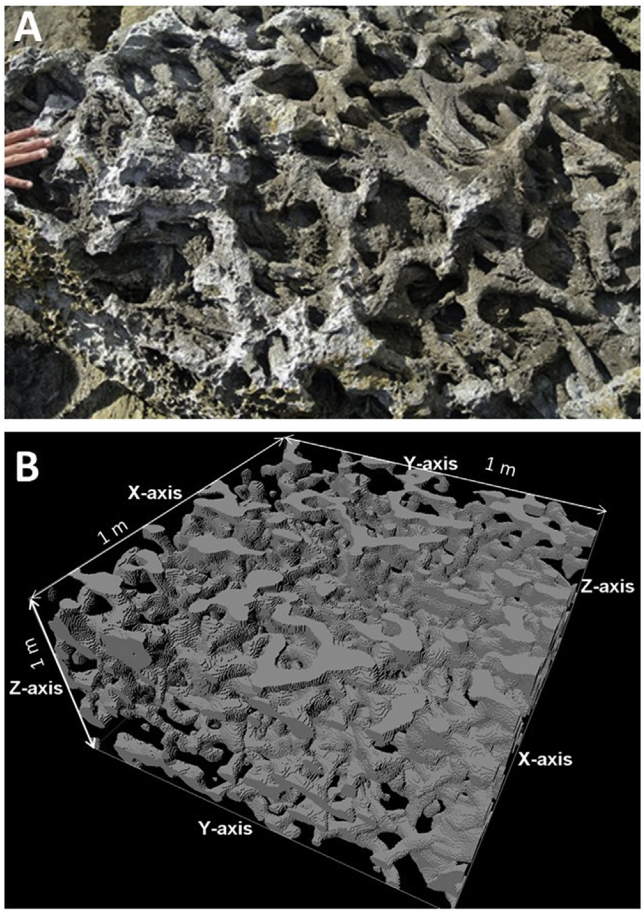

Fig. 1. Qualitative comparison between TBN in an outcrop and in the model. (A) Outcrop photograph showing 3D view of TBN after the burrow matrix has been washed out. Outcrop of Birdsall Calcareous Grit Member of the Coralline Oolite Formation, Upper Jurassic, Oxfordian, England) from the website http://woostergeologists.scotblogs.wooster.edu/tag/uk2015/page/3/. Note hand for scale. (B) Filtered 3D models based on TBN with 30% intensity. Note that TBN of outcrop and models include similar morphological patterns.

from the constructed TBN model (Fig. 2D–G). Although the TBN in our models is larger, these models and core CT scan share similar 2D morphology of the TBN. This similarity in connectivity pattern in TBN models of our study and stratigraphic record suggest reasonable approximation of TBN morphology for the models and, consequently, connectivity, and flow simulation modeling results.

3.2. 3D models and connectivity of TBN

The 15 3D models representing different TBN burrow intensities capture a range of characteristics of connected burrows and hence connected porosity. Qualitative visual results showing volumes of connected TBN (Fig. 3A–D) illustrate that at low intensity (2%), many small isolated bodies are present (Fig. 3A). As intensity increases (8%), connected bodies become larger and more numerous (Fig. 3B). At 12% intensity, the largest body includes a vast majority of the total burrow network volume (grey color in Fig. 3C), and by 50%, almost all of the burrows are connected (Fig. 3D).

These patterns can be quantified by comparing burrow intensity and connectivity. To assess connectivity, the largest TBN volume is expressed as the ratio of the largest burrow volume to the total burrow network volume, expressed as a percentage. With this metric, the higher the percentage, the more connected the TBN. The data (Fig. 3E) reveal that the connectivity of TBN in the 3D models increases with bioturbation intensity, but that this increase is nonlinear. The crossplot of burrow intensities versus largest TBN volumes (Fig. 3E) reveals three general classes, each with distinct patterns of connectivity.

The first class, which represents low ii (ii2, TBN of 2–10%, Fig. 3A, E) has isolated TBN volumes, and the largest volume is < 40% of the total burrow volume. In the second class, which has low to intermediate bioturbation intensity (ii3, TBN range from 12 to 20%), > 85% of TBN is connected in the largest volume (Fig. 3B, C, E). There are, however, in this class some TBN volumes that are not connected to the largest volume. The third class, which represents high ii (ii3, 5, TBN range 30–70%), consists essentially of one connected TBN volume that includes > 99% of total burrow volume (Fig. 3D and E).

3.3. Property models and upscaled models of TBN

As facies-based models, the distribution of porosity and permeability in the TBN models is consistent with their geometrical patterns, and TBN show interconnected permeable pathways that increase in connectivity with increased burrow density. Nonetheless, as cell size increases through upscaling of models (Table 1), the geometrical details, and porosity and permeability distribution, of the TBN change considerably (Fig. 4).

This smoothing is captured in the measures of petrophysical properties (range, variance, and standard deviation of porosity and permeability) in upscaled TBN models. The results illustrate that the mean stays the same, but the range and variance decrease with increasing cell size of the models, marking increasing homogenization of these properties with upscaling (Fig. 4). Whereas the fine-grid models (Fig. 4A–E) preserve the geometrical details (Fig. 4A–E) of the TBN, the coarse-grid models (Fig. 4F–J) show homogenization between the TBN and matrix (Fig. 4F–J). The visual inspection of models and the permeability data in the upscaled models both demonstrate this trend (Figs. 5 and 6). The upscaled model with 20,000 cells has the smallest number of cells that preserves the geometry of TBN (Fig. 4E) and retains most of the range and variance in petrophysical properties (Fig. 5) and, therefore, was selected for flow simulation runs.

3.4. Fluid flow simulation

Fluid-flow simulations run on upscaled models included 20,000 cells and continued until water breakthrough in the production well (Fig. 6). The data for all simulation runs show qualitatively similar trends—initial increase in production (Fig. 6A), pressure and cumulative gas production (Fig. 6B) to a certain point at which pressure and rate decrease, and water production rate markedly increases (four representative examples is illustrated in Fig. 6A). The time of water breakthrough depends on the TBN burrow intensity (Fig. 6A, the higher the TBN burrow intensity, the slower the water breakthrough occurs). In models with TBN burrow intensity > 50%, however, water breakthrough occurs at a faster rate than in models with TBN burrow intensity > 50%.

Fifteen simulation cases were run for each of the simulation conditions (condition 1–3, Fig. 7B) and the results were compared on a plot of TBN intensity versus cumulative GPC (Fig. 7):

- Condition 1 (Table 3, Fig. 7A and B): The models yielded insignificant gas volume. 12 out of 15 models have GPC < 0.1 SM^3, whereas the other three models have GPC < 2.4 SM^3.
- Condition 2 (Table 3, Fig. 7A and B): The models with TBN burrow intensity < 30% (10 models) have considerable gas production (GPC < 0.1 SM^3) whereas the ones with burrow intensity > 30% (5 models) yielded significant gas production (GPC > 11 SM^3). GPC increase steadily with increase of TBN burrow intensity in the models with burrow intensity > 30%.
- Condition 3 (Table 3, Fig. 7A and B): The models started yielding gas from relatively low TBN burrow intensity. GPC of the models show nonlinear increases with increased TBN intensity, and can be

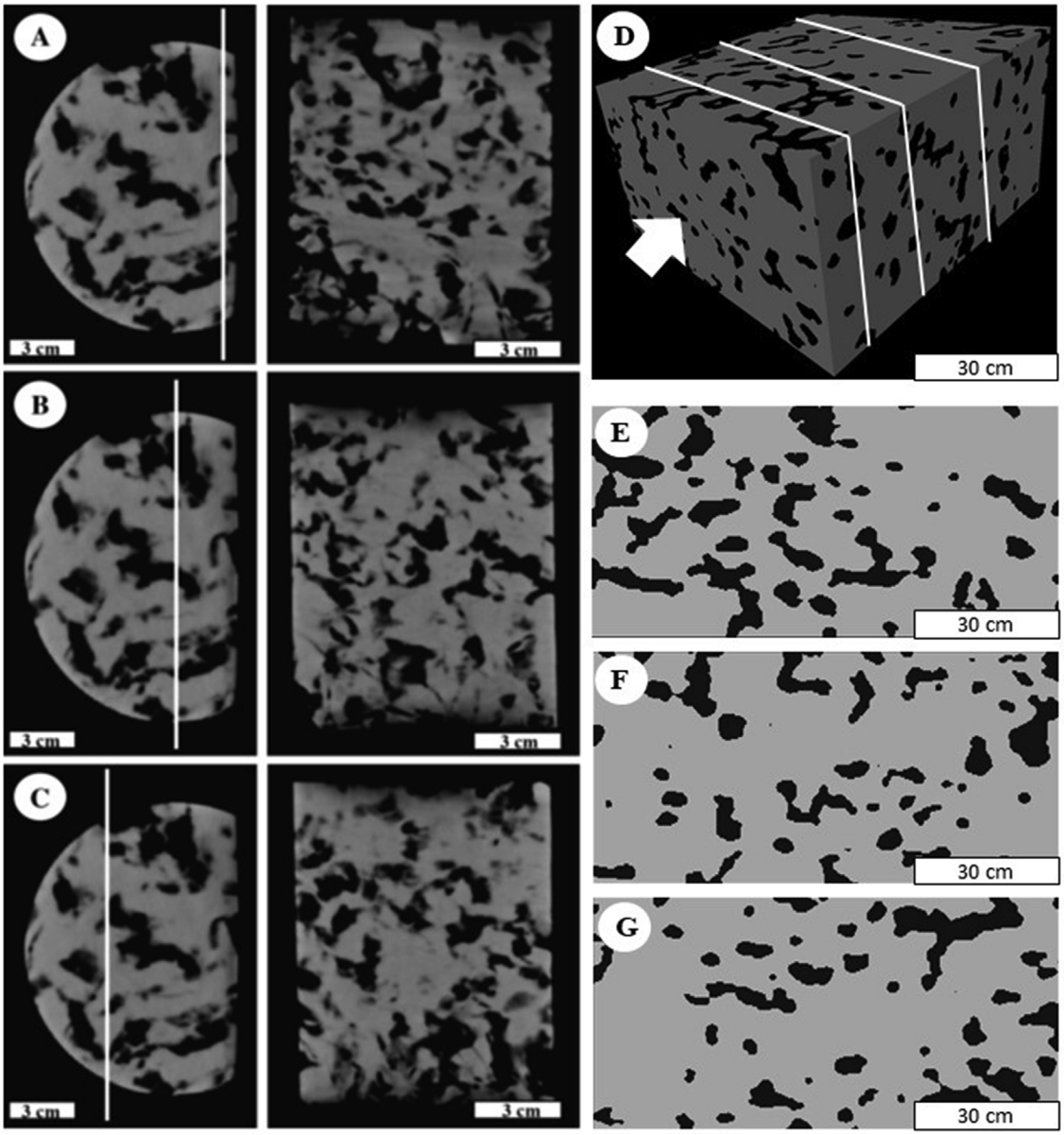

Fig. 2. Comparison between TBN in a subsurface reservoir and in the model. (A–C) 2D helical-CT scans perpendicular to the top of a bioturbated core sample (Baniak et al., 2013). On the left side are three identical 2D photos (top of core) indicating location of cross-sectional slices for 2D CT analysis (vertical white lines). (D–G) 2D slices from TBN model of 20% burrow intensity. (D) White lines indicate location of the 2D slices. Note similar 2D morphology of TBN despite the difference in burrow size.

linked to connectivity pattern of TBN (Fig. 3E). Most importantly in this condition, models with TBN > 50% exhibited early water breakthrough (Fig. 6).

4. Discussion

The models successfully recreate patterns similar to the real-world outcrop and subsurface TBN (Figs. 1 and 2). These models provide first-order insights into several aspects of bioturbated reservoirs, including network connectivity, relations between burrows and matrix, and, ultimately, fluid flow in these systems.

4.1. TBN connectivity

The 3D modeling results suggest that elevated connectivity of TBN in firmgrounds can be established at relatively low bioturbation intensity (ii3, at ~12%, Fig. 1). Thus, TBN in the *glossifungites* ichnofacies can provide a connected permeable pathway for flow, even at a low level of bioturbation, if burrows are filled with permeable sediment. This result is consistent with previous studies (e.g., La Croix et al., 2012), in which computer models of *Thalassinoides* assessed the impact of bioturbation on petrophysical properties. Their results indicated that at 10% intensity TBN, 90% of the network could be connected.

The 12% intensity corresponds to the lower range of ii3 (Droser and Bottjer, 1986), and in many cases, this intensity could be underappreciated as providing nearly full connectivity for TBN. The possible reason for this underestimation is that TBN either in core and outcrop with 10–30% in 2D view do not appear to be connected, and suggest (incorrectly) that many burrows are isolated (Fig. 8A and B). The 3D models of TBN in this study, however, reveal that even at this low intensity, a well-established framework can be established (Fig. 8C).

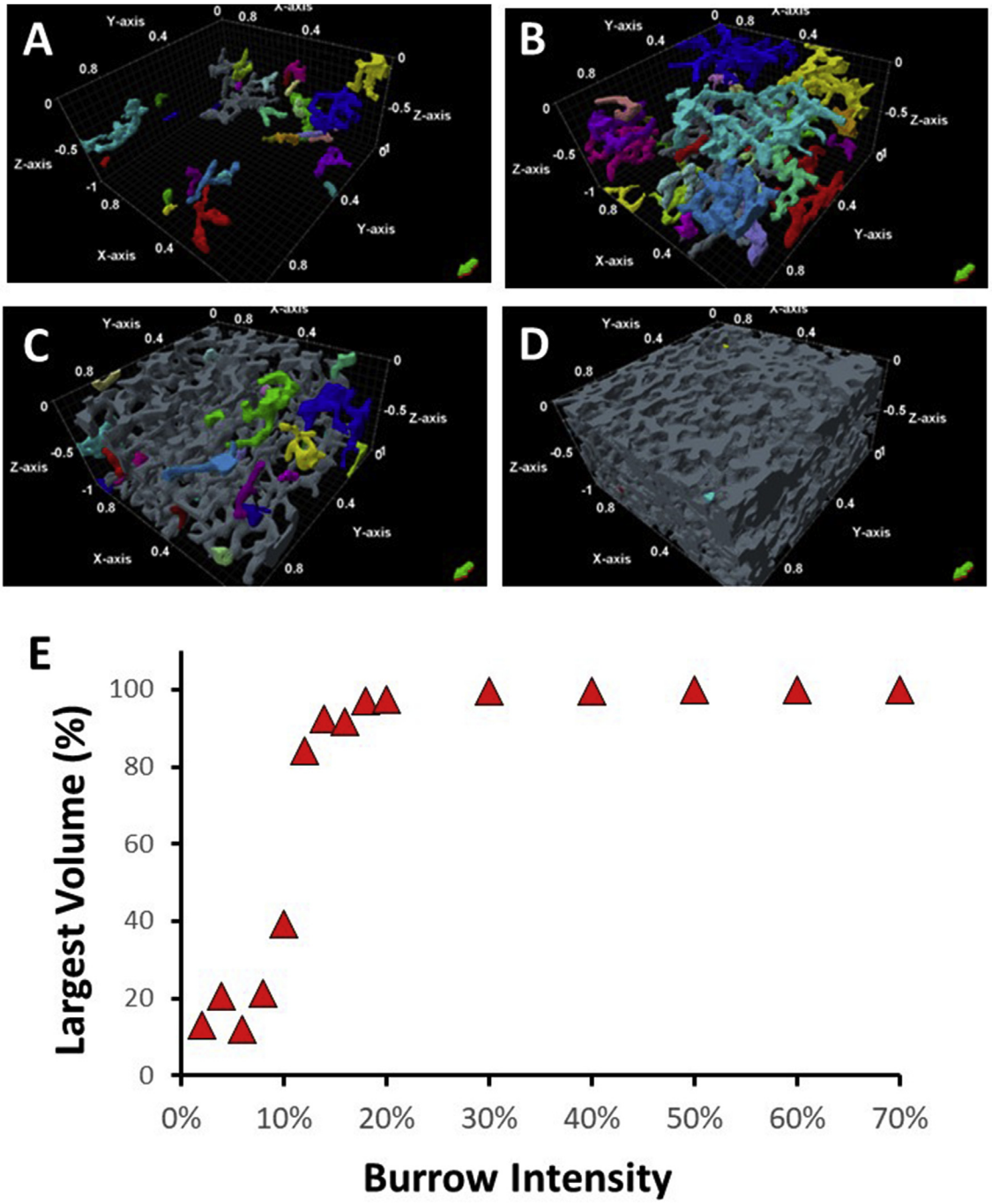

Fig. 3. 3D models based on TBN. (A–D) Four filtered 3D models based on TBN for 2%, 8%, 12%, and 30%, respectively; bodies of a similar color represent distinct connected volumes. Note that TBN show isolated volumes at intensity 2% (part A), but expand to roughly 85% connectivity at bioturbation intensity of 12% (part C). (E) Crossplot bioturbation intensity versus volume of largest TBN (expressed as % of total TBN) in the 15 models. Note the sharp increase in connected volumes from 0 to 12% intensity, but that above 12%, almost all volumes are connected. (For interpretation of the references to color in this figure legend, the reader is referred to the Web version of this article.)

4.2. The effect of interaction between TBN and matrix on fluid flow

Comparing results among fluid flow simulation conditions (condition 1–3, Table 3) constrains the role of petrophysical properties of the matrix and TBN as two end members responsible for the flow properties in bioturbated beds. The results indicated that mud-dominated matrix has low capacity to produce gas if the permeability of TBN is assigned to zero (production is not more than 2.4 SM^3, condition 1, Table 3). On the other hand, production from TBN alone (matrix assigned zero permeability) indicated that TBN-bearing strata produce only at burrow intensity < 30% (see data of condition 2, Table 3 and Fig. 7B). Interestingly, in situations in which both matrix and TBN contribute to the gas production (condition 3, Table 3 and Fig. 7B), the production of gas is enhanced markedly. The interaction between matrix and TBN seems to connect more TBN bodies, and increase their production, and likely h[illegible] gas diffusion from matrix through TBN. This interpretation s[illegible]hat GPC in the TBN models controlled primarily by TBN con-n[illegible] and matrix permeability, and that these TBN models represent dual porosity fluid flow category of Gingras et al. (2012).

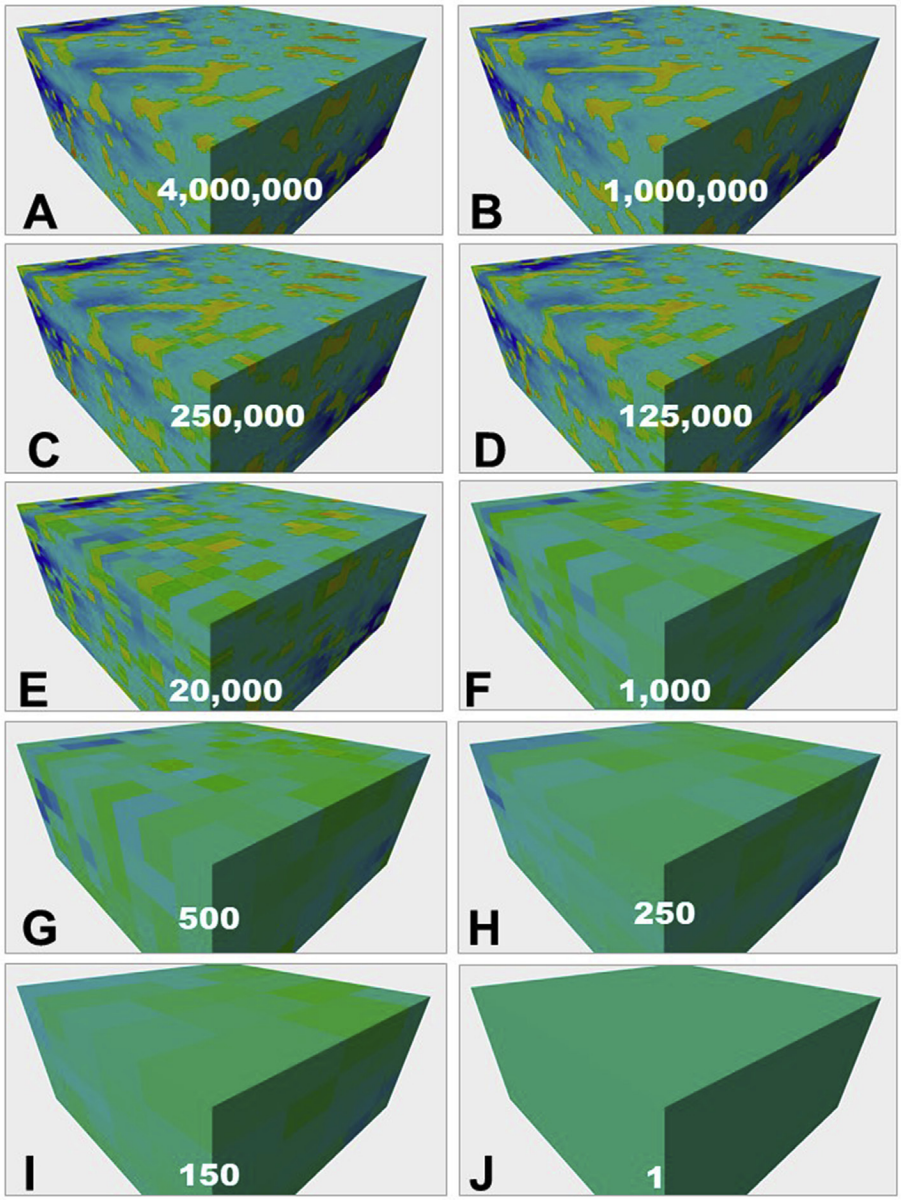

Fig. 4. Sequential, upscaled permeability models of TBN with 10% intensity. Numbers represent the number of voxels in the model. Note how details of TBN (and their distinct permeabilities) decrease gradually from fine grid models to coarse grid models.

4.3. Fluid flow from TBN and matrix

The results of fluid flow simulation in condition 3 (production from both TBN and burrow matrix) suggest that flow rate in bioturbated reservoirs respond differently to TBN intensity (Fig. 7C). TBN models at intensities from 2% to 10% had a variable flow rate, differences possibly related to the random arrangement of (relatively rare) TBN volumes in the 3D model at these low intensities. That is, production depends largely on the connection of a large TBN volume to the well. These relations are illustrated in the models of TBN = 4% and 8% intensity (Fig. 7C). In the 4% burrow intensity model, although the entire TBN volumes in the model are not connected, they are penetrated by the production well, and cumulative production is 5 SM^3/Day. In models of TBN of 8%, TBN volumes were not penetrated by the well, and as a result, the model yielded zero production.

TBN models of intensity from 10% to 20% have flow rate that increases with TBN intensity. The relationship is not linear, however, likely because the unconnected volumes of TBN at these intensities affect production rate. The incremental increase in flow rate with step increase in bioturbation intensity between 20% and 50% is greater than that in models of TBN > 50%. Deviation from linearity in these intensities can be attributed to the presence of one large volume of connected TBN in intensity > 50%, a feature that resulted in the formation of high-permeability conduits. In these possibilities, water breakthrough occurs faster than in models with burrow intensity < 50% (Fig. 7A). This situation is common (at a larger scale) in production settings where bottom water infiltrates the perforation zone rapidly and results in a super-permeability (super-k) zone and reduces hydrocarbon production. In the case of our model, water breakthrough reduces gas production. Nonetheless, in contrast to the negative impact on model production (a model with a limited hydrocarbon in place), in real-world bioturbated reservoirs, this type of super-k pathway could enhance production, at least for some period of time before water breakthrough. For example, “super-k” zones of Arab-D reservoir in Saudi Arabia that have been interpreted to reflect *Thalassinoides*-bioturbated strata (ii3–ii4, Pemberton and Gingras, 2005) may represent comparable

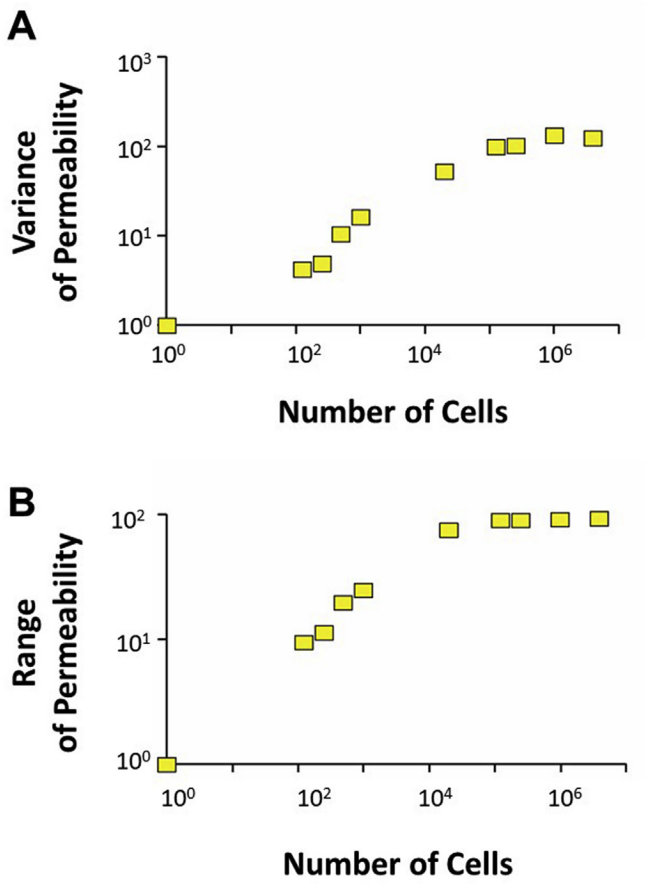

Fig. 5. Crossplots showing permeability (A) variance, and (B) range of permeability versus number of cells in the sequentially upscaled models. Note marked decrease in range and variance of permeability in models with less than 20,000 cells.

flow.

4.4. Comparison with previous studies

Recent efforts to numerically model trace fossils in reservoir rock used computer simulations and have demonstrated how trace-fossil connectivity can enhance reservoir flow unit in bioturbated reservoirs (Pemberton and Gingras, 2005; Tonkin et al., 2010; Gingras et al., 2012; La Croix et al., 2012; Baniak et al., 2013, 2015; Bayet-Goll et al., 2017; Leaman and McIlroy, 2017; Uddin et al., 2017). This study takes the next logical steps enhancing the workflow of burrow interconnectivity and numerical modeling in several ways. First, the use of MPS allowed for reproduction of intensity and connectivity variation of TBN in a bioturbated reservoir, resulting in geometrical patterns similar to real-world carbonate outcrops. Second, the use of a random function to distribute porosity and permeability values in each cell of the numerical models allowed for more realistic petrophysical distribution than assigning a single value of porosity and permeability for the burrow network and a signal value of porosity and permeability for the medium as in previous work (e.g., Baniak et al., 2013). Third, the use of multicellular grids for TBN models allowed us to understand the effect of upscaling on the preservation of TBN geometry and their petrophysical properties. Fourth, the numerical models provide a useful purview to perform such advanced steps as running a flow-fluid simulation on TBN to understand their flow-rate variation with burrow intensity.

Besides using these advanced steps of TBN modeling and simulation, this study honored morphological shapes to build the MPS models, resulting in realistic networks comparable to the morphology of *Thalassinoides* burrows (e.g., Ekdale and Bromley, 1984; Pemberton and Gingras, 2005; La Croix et al., 2012; Rodríguez-Tovar et al., 2017). This morphology has two major components: 1) the boxwork pattern; and 2) the circular to subcircular segments of the tunnels and shafts. Both may have an impact on the results.

Among different trace fossils, connectivity trends related to burrow intensity likely will be different because of morphological differences; as a result, the connectivity patterns of TBN may not be directly applicable to other trace fossils. For example, *Skolithos* is a vertical tube with no lateral branches (e.g., Alpert, 1974; Häntzschel, 1975; Droser and Bottjer, 1993). Such morphology would only have a vertical component of connectivity, which would be completely different than TBN. *Phycosiphon* is a small, oblique or parallel to bedding, spreiten-filled burrow system comprised of protrusive U-shaped lobes with dark, fine-grained cores and light, coarser grained mantles (e.g., Wetzel and Bromley, 1994; Gluszek, 1998). Such morphology would be expected to have a much smaller vertical and horizontal connectivity than *Thalassinoides* (e.g., Naruse and Nifuku, 2008; Bednarz and McIlroy, 2012).

The morphological variation of burrows which usually results in a different pattern of burrow connectivity can impact permeability anisotropy, and thus, directions of flow. Therefore, average permeability of bioturbated reservoir (arithmetic [horizontal], geometric [isotropic], and harmonic [vertical] average permeability) can vary considerably with the morphological variation of burrows (Gingras et al., 1999; La Croix et al., 2013, 2012). Our models assume a homogeneous distribution of TBN, which simplifies the role of permeability anisotropy. Future work is needed on these models to understand the role of permeability anisotropy related to burrow morphology.

Not only the burrow morphology which affects permeability anisotropy, but also burrow intensity. Work by Baniak et al. (2013, 2015) showed examples where bulk permeability is best estimated using the geometric mean at low to moderate volumes of burrow dolomite (25–65%) and arithmetic mean at high volumes of burrow dolomite (65–80%). Within dual-permeability models, bulk permeability is best estimated using the geometric mean at low to moderate volumes of burrow dolomite (10–50%) and arithmetic mean at moderate to high volumes of burrow dolomite (50–80%). Future works adopting the workflow presented in this study should take into account these variations.

In addition to the morphology, orientation, and intensity, burrow infill is an important factor for determining the effective flow properties of TBN. Our models simulate TBN infill that consists of coarse (porous and permeable) sediment. Although this assumption is analogous to many *Thalassinoides*-bearing strata (e.g., Carvalho et al., 2007), in other cases, TBN could have fine, nonporous, nonpermeable sediment infill (e.g., Jin et al., 2012). Such infill—with little or no porosity or permeability—could result in zero flow. Thus, a careful sedimentological and ichnological investigation should be conducted before modeling TBN to understand the flow properties of any particular reservoir.

Spot-permeability measurements provide useful information to understand burrow infill in TBN permeability (e.g., Tonkin et al., 2010; Gingras et al., 2012). Upscaling these measurements in grids with cell sizes large enough (models with cell size > 10 cm; Fig. 4F–J) to homogenize TBN geometry and permeability, however, represent the main challenge for reservoir modeling of TBN strata. As indicated in here, TBN may enhance permeability, but upscaling TBN models also could result in an overestimation of hydrocarbon in place and cumulative flow rates. Thus, the question of what is the appropriate porosity and permeability for reservoir modeling of TBN strata should be answered, but this topic needs more investigation.

5. Conclusions

The general notion that burrow connectivity can enhance permeability is furthered and advanced by geostatistical modeling of burrow connectivity of TBN. Results enhance quantitative understanding of the

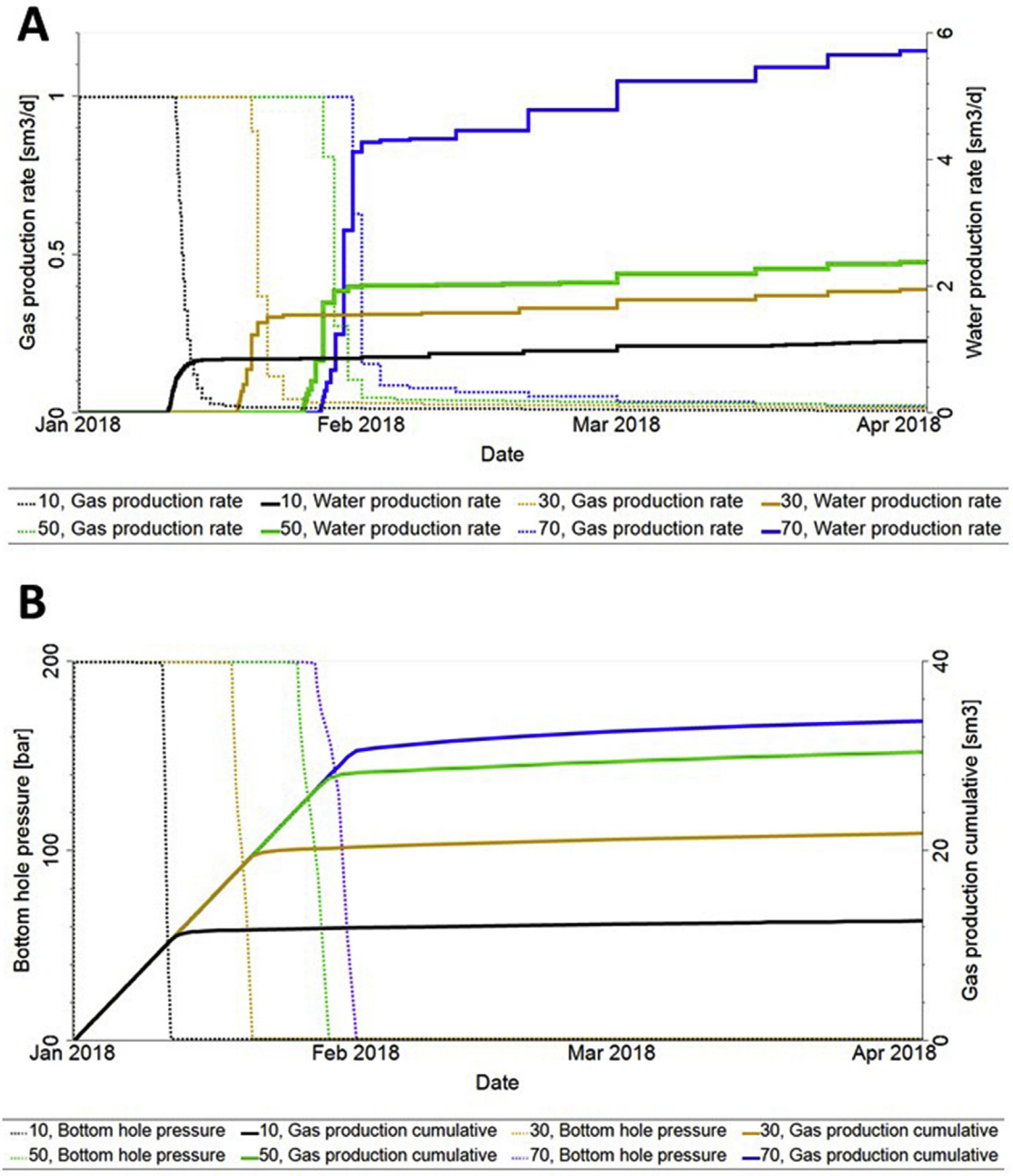

Fig. 6. Simulation of flow results. Representative simulation results showing example from condition 3 (producing from both burrow matrix and TBN) with TBN intensity of 10%, 30%, 50% and 70%. Note that (A) water breakthrough and (B) drop of bottom hole pressure defines the end of gas production. Note also the early water breakthrough in model with 70% of TBN which is interpreted as evidence of super k.

relationships between burrow intensity and burrow connectivity. The study further quantifies the impact of burrow intensity on hydrocarbon productivity, insights useful to predict how flow rate could vary with burrow intensity in analogous bioturbated carbonate reservoirs. Key findings of this study are:

- 2D TBN models mimicking common core and outcrop views incorrectly suggest that many burrows are isolated. Nevertheless, 3D TBN models reveal that burrow connectivity depends on burrow intensity, and that a well-established, connected framework can be recognized with as little as 12% burrow intensity.
- TBN have a fluid-flow rate controlled primarily by TBN connectivity and matrix permeability.
- TBN have a fluid-flow rate that increases nonlinearly with burrow intensity, with the rate controlled primarily by TBN connectivity, and that early breakthrough can occur at high intensity (TBN > 50%).
- The interaction between matrix and TBN seems to connect more isolated TBN bodies, and increase GPC, and likely help the gas diffusion from matrix through TBN.

Acknowledgments

We acknowledge the Donors of the American Chemical Society Petroleum Research Fund for partial support of this research, to the sponsors of the Kansas Interdisciplinary Carbonates Consortium (KICC) for partially supporting this study, and to Schlumberger for providing free license for Petrel. Thanks L. Buatois the Associate Editor of Marine

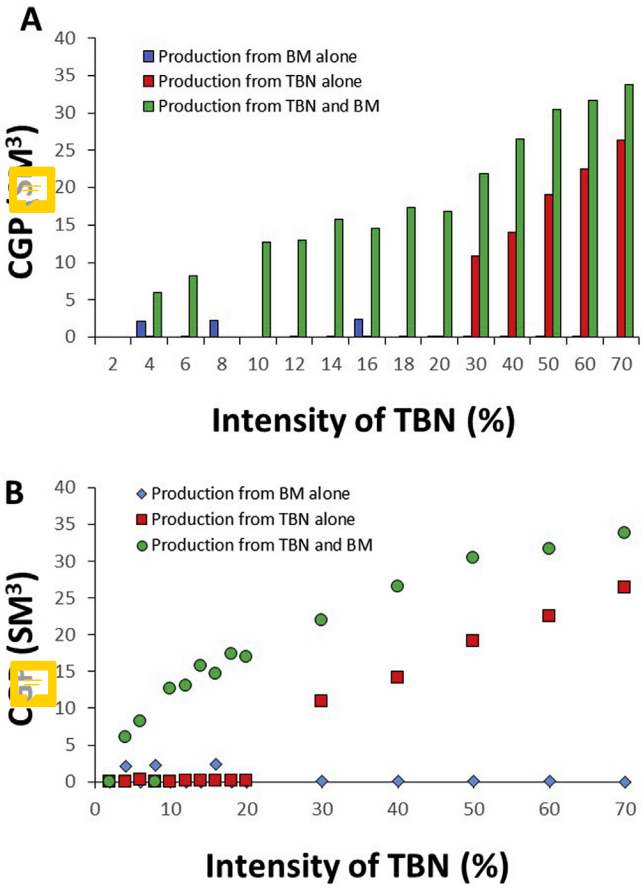

Fig. 7. Cumulative gas production (GPC) results for the three simulation conditions. Condition 1: production from burrow matrix (BM) alone; condition 2: production from TBN alone; condition 3: production from both BM and TBN. (A) Bar chart showing variability among GPC of the three simulation conditions. (B) GPC plotted based on TBN percentages for each simulation condition.

Table 3
Results of the three-conditions simulations.

Simulation Case	TBN %	Condition 1		Condition 2		Condition 3	
		Production from BM only		Production fromTBN only		Production from both TBN & BM	
		GIP	GPC	GIP	GPC	GIP	GPC
1	2	1.82	0.00	0.68	0.00	2.67	0.00
2	4	2.44	2.16	1.38	0.01	6.80	5.74
3	6	2.77	0.00	2.18	0.18	9.73	8.22
4	8	2.50	2.26	2.45	0.00	9.42	0.00
5	10	2.43	0.00	4.13	0.00	13.97	12.68
6	12	2.05	0.00	4.64	0.03	14.18	13.03
7	14	1.45	0.00	5.64	0.03	17.07	15.72
8	16	2.52	2.37	5.92	0.05	16.00	14.64
9	18	1.55	0.00	6.93	0.02	18.69	16.88
10	20	1.43	0.00	6.87	0.07	18.54	17.39
11	30	1.45	0.05	11.59	10.81	23.98	21.90
12	40	0.78	0.04	15.15	14.09	28.91	26.48
13	50	0.69	0.12	20.59	19.06	33.55	30.49
14	60	0.49	0.10	24.13	22.53	34.61	31.67
15	70	0.26	0.00	27.63	26.33	35.72	33.76

GIP: Gas-in-place.
GPC: Cumulative gas production.
Burrow matrix: BM.
Thalassinoides burrow networks: TBN.

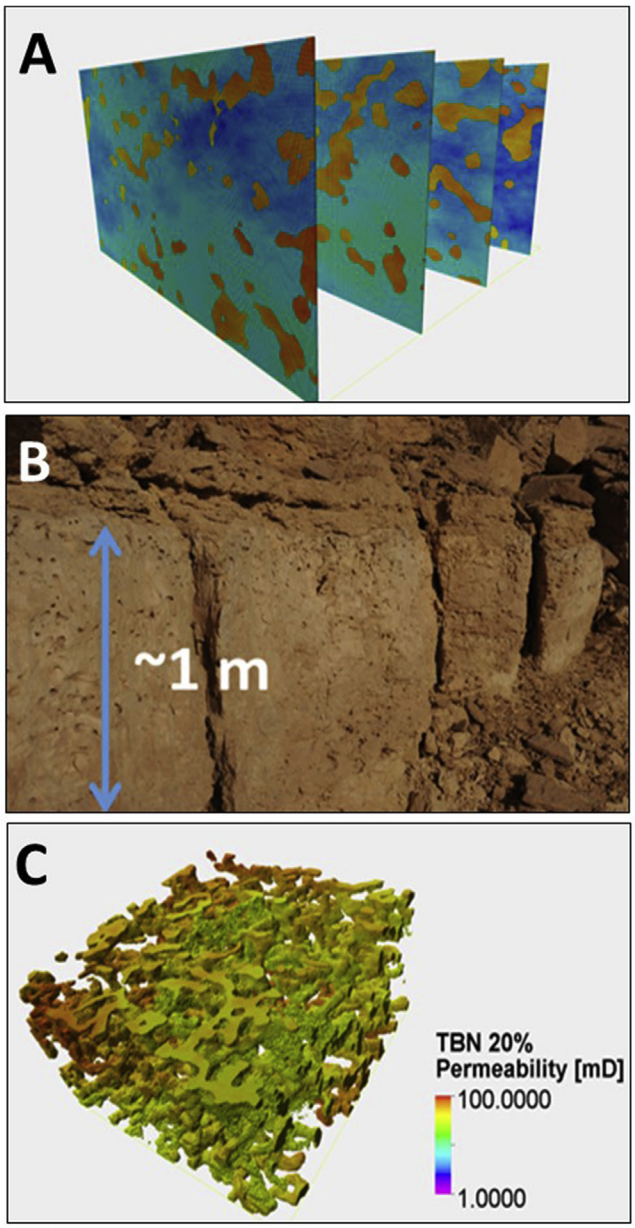

Fig. 8. Representations of TBN in 2D. (A) Vertical 2D panels of TBN model with 20% intensity. (B) Photograph of representative face of outcrop with TBN (Eltom et al., 2018). In A and B note that TBN appear as isolated bodies in 2D view. (C) Filtered 3D models based on TBN with 20% intensity showing that TBN is highly connected (unlike what appears in 2D views).

and Petroleum Geology, G. Baniak, and the anonymous reviewer for the valuable comments on this paper.

Appendix A. Supplementary data

Supplementary data to this article can be found online at https://doi.org/10.1016/j.marpetgeo.2019.03.019.

References

Alpert, S.P., 1974. Systematic review of the genus Skolithos. J. Paleontol. 48, 661–669.
Baniak, G.M., Gingras, M.K., Pemberton, S.G., 2013. Reservoir characterization of burrow-associated dolomites in the Upper Devonian Wabamun Group, Pine Creek gas field, central Alberta, Canada. Mar. Petrol. Geol. 48, 275–292.
Baniak, G.M., Gingras, M.K., Burns, B.A., Pemberton, S.G., 2015. Petrophysical characterization of bioturbated sandstone reservoir facies in the upper jurassic Ula Formation, Norwegian North Sea, Europe. J. Sediment. Res. 85 (1), 62–81.

Bayet-Goll, A., Samani, P.N., de Carvalho, C.N., Monaco, P., Khodaie, N., Pour, M.M., Kazemeini, H., Zareiyan, M.H., 2017. Sequence stratigraphy and ichnology of early cretaceous reservoirs, Gadvan formation in southwestern Iran. Mar. Petrol. Geol. 81, 294–319.

Bednarz, M., McIlroy, D., 2012. Effect of phycosiphoniform burrows on shale hydrocarbon reservoir quality. AAPG Bull. 96 (10), 1957–1980.

Cunningham, K.J., Sukop, M.C., Huang, H., Alvarez, P.F., Curran, H.A., Renken, R.A., Dixon, J.F., 2009. Prominence of ichnologically influenced macroporosity in the karst Biscayne aquifer: Stratiform "super-K" zones. Geol. Soc. Am. Bull. 121 (1–2), 164–180.

Carvalho, C.N.D., Viegas, P.A., Cachão, M., 2007. *Thalassinoides* and its producer: populations of *Mecochirus* buried within their burrow systems, Boca do Chapim Formation (Lower Cretaceous), Portugal. Palaios 22 (1), 104–109.

Droser, M.L., Bottjer, D.J., 1986. A semiquantitative field classification of ichnofabric. J. Sediment. Res. 56 (4), 558–569.

Droser, M.L., Bottjer, D.J., 1993. Trends and patterns of Phanerozoic ichnofabrics. Annu. Rev. Earth Planet Sci. 21 (1), 205–225.

Ekdale, A.A., Bromley, R.G., 1984. Sedimentology and ichnology of the Cretaceous-Tertiary boundary in Denmark: implications for the causes of the terminal Cretaceous extinction. J. Sediment. Res. 54 (3), 681–703.

Eltom, H.A., Gonzalez, L.A., Hasiotis, S.T., Rankey, E.C., Cantrell, D.L., 2018 Feb 1. Paleogeographic and paleo-oceanographic influences on carbon isotope signatures: implications for global and regional correlation, Middle-Upper Jurassic of Saudi Arabia. Sediment. Geol. 364, 89–102.

Eltom, H., Hasiotis, S.T., 2017 May. Lateral and vertical trends of preferred flow pathways associated with bioturbated carbonate: examples from Middle to Upper Jurassic strata, central Saudi Arabia. In: McNeill, D., Harris, P.M., Rankey, E., Hsieh, J. (Eds.), Carbonate Pore Systems: New Developments and Case Studies. Special Publication 112: SEPM (Society for Sedimentary Geology), Tulsa, Oklahoma.

Gingras, M.K., Baniak, G., Gordon, J., Hovikoski, J., Konhauser, K.O., La Croix, A., Lemiski, R., Mendoza, C., Pemberton, S.G., Polo, C., Zonneveld, J.P., 2012. Porosity and permeability in bioturbated sediments. In: Developments in Sedimentology, vol 64. Elsevier, pp. 837–868.

Gluszek, A.R., 1998. Trace fossils from late Carboniferous storm deposits, upper Silesia coal basin, Poland. Acta Palaeontol. Pol. 43 (3), 517–546.

Häntzschel, W., 1975. *Trace fossils and Problematica* (2nd edition). In: Teichert, C. (Ed.), Treatise on Invertebrate Paleontology, Part W. Miscellanea, Suppl. 1. Geological Society of America and University of Kansas Press, Boulder, Colorado, pp. 269.

Jin, J., Harper, D.A., Rasmussen, J.A., Sheehan, P.M., 2012. Late Ordovician massive-bedded *Thalassinoides* ichnofacies along the palaeoequator of Laurentia. Palaeogeogr. Palaeoclimatol. Palaeoecol. 367, 73–88.

La Croix, A.D., Gingras, M.K., Dashtgard, S.E., Pemberton, S.G., 2012. Computer modeling bioturbation: the creation of porous and permeable fluid-flow pathways. Amer. Assoc. Petrol. Geolog. Bull. 96 (3), 545–556.

La Croix, A.D., Gingras, M.K., Pemberton, S.G., Mendoza, C.A., MacEachern, J.A., Lemiski, R.T., 2013. Biogenically enhanced reservoir properties in the Medicine Hat gas field, Alberta, Canada. Mar. Petrol. Geol. 43, 464–477.

Leaman, M., McIlroy, D., 2017. Three-dimensional morphological and permeability modelling of *Diplocraterion*. Ichnos 24 (1), 51–63.

Meyer, F.O., Price, R.C., Al-Raimi, S.M., 2000. Stratigraphic and petrophysical characteristics of cored Arab-D super-k intervals, Hawiyah area, Ghawar field, Saudi Arabia. GeoArabia 5 (3), 355–384.

Naruse, H., Nifuku, K., 2008. Three-dimensional morphology of the ichnofossil *Phycosiphon incertum* and its implication for paleoslope inclination. Palaios 23 (5), 270–279.

Pemberton, S.G., Gingras, M.K., 2005. Classification and characterizations of biogenically enhanced permeability. Amer. Assoc. Petrol. Geolog. Bull. 89 (11), 1493–1517.

Rodríguez-Tovar, F.J., Miguez-Salas, O., Duarte, L.V., 2017. Toarcian Oceanic Anoxic Event induced unusual behaviour and palaeobiological changes in *Thalassinoides* tracemakers. Palaeogeogr. Palaeoclimatol. Palaeoecol. 485, 46–56.

Tonkin, N.S., McIlroy, D., Meyer, R., Moore-Turpin, A., 2010. Bioturbation influence on reservoir quality: a case study from the Cretaceous Ben Nevis Formation, Jeanne d'Arc basin, offshore Newfoundland, Canada. AAPG (Am. Assoc. Pet. Geol.) Bull. 94 (7), 1059–1078.

Uddin, Y.N., Clerke, E.A., Bammel, B., Koronfol, S., Grader, A., 2017 May. Quantitative study of formation vertical permeability in Middle East *Thalassinoides* burrowed carbonate mudstone. In: SPE Reservoir Characterisation and Simulation Conference and Exhibition. Society of Petroleum Engineers.

Wetzel, A., Bromley, R.G., 1994. Phycosiphon incertum revisited: anconichnus horizontalis is its junior subjective synonym. J. Paleontol. 68 (6), 1396–1402.